

Synthesis and Characterization of $K_{8-x}(H_2)_ySi_{46}$

Doinita Neiner,[†] Norihiko L. Okamoto,[‡] Ping Yu,[§] Sharon Leonard,[†] Cathie L. Condon,^{||} Michael F. Toney,^{||} Quentin M. Ramasse,[⊥] Nigel D. Browning,^{‡,⊥,#} and Susan M. Kauzlarich^{*†}

[†]Department of Chemistry, [‡]Department of Chemical Engineering and Materials Science, and [§]NMR Facility, University of California, One Shields Avenue, Davis, California 95616, ^{||}Stanford Synchrotron Radiation Lightsource, SLAC National Accelerator Laboratory, Menlo Park, California 94025, [⊥]National Center of Electron Microscopy, Lawrence Berkeley Laboratory, 1 Cyclotron Road, Berkeley, California 94270, and [#]Physical and Life Sciences Directorate, Lawrence Livermore National Laboratory, Livermore, California 94550

Received March 9, 2009

A hydrogen-containing inorganic clathrate with the nominal composition, $K_7(H_2)_3Si_{46}$, has been prepared in 98% yield by the reaction of K_4Si_4 with NH_4Br . Rietveld refinement of the powder X-ray diffraction data is consistent with the clathrate type I structure. Elemental analysis and 1H MAS NMR confirmed the presence of hydrogen in this material. Type I clathrate structure is built up from a Si framework with two types of cages where the guest species, in this case K and H_2 , can reside: a large cage composed of 24 Si, in which the guest resides in the $6d$ position, and a smaller one composed of 20 Si, in which the guest occupies the $2a$ position (cubic space group $Pm\bar{3}n$). Potassium occupancy was examined using spherical aberration (Cs) corrected scanning transmission electron microscopy (STEM). The high-angle annular dark-field (HAADF) STEM experimental and simulated images indicated that the K is deficient in both the $2a$ and the $6d$ sites. 1H and ^{29}Si MAS NMR are consistent with the presence of H_2 in a restricted environment and the clathrate I structure, respectively. FTIR and $^{29}Si\{^1H\}$ CP MAS NMR results show no evidence for a Si–H bond, suggesting that hydrogen is present as H_2 in interstitial sites. Thermal gravimetry (TG) mass spectrometry (MS) provide additional confirmation of H_2 with hydrogen loss at ~ 400 °C.

Introduction

Clathrates constitute a unique class of inclusion compounds with a rich crystal chemistry that allows for a variety of physical properties such as thermoelectricity, superconductivity, and hydrogen storage.^{1–3} The crystal structure of clathrates consists of three-dimensional host frameworks that encapsulate different guest molecules.^{4,5} The framework is formed of polyhedra with pentagonal and/or hexagonal faces. The variation in these structures arises from the type of polyhedra that host atoms form and the polyhedra connectivity.^{4–6} Among the numerous structure types of the inorganic clathrate compounds, type I and type II clathrates

have been very extensively investigated. Most of type I clathrates, M_8T_{46} , crystallize in $Pm\bar{3}n$, cubic cell consisting of two dodecahedra (T_{20} cage) and six tetrakaidecahedra (T_{24} cage) encapsulating guests (M) at $2a$ and $6d$ sites. Type II clathrates, $M_{24}T_{136}$, have a cubic cell, $Fd\bar{3}m$, made of pentagonal dodecahedra (T_{20}) and hexakaidecahedra (T_{28}) while the 24 guest atoms M, occupy $8b$ and $16c$ positions.^{6,7} An illustration of the different clathrate cages in Type I is presented in Figure 1. The $6d$ site is shaded.

Inorganic clathrates (type I and II) in which group 14 elements make up the framework structure and alkali metals reside in the guest sites have been studied for their possible thermoelectric applications.^{2,3,5,8} The type II clathrate hydrates in which H_2O molecules comprise the framework structure with H_2 molecules as the guest species have been of interest for hydrogen storage applications.^{1,9} We have reported the synthesis of a new type-I Si clathrate,

*To whom correspondence should be addressed. E-mail: smkauzlarich@ucdavis.edu.

(1) Lee, H.; Lee, J. W.; Kim, D. Y.; Park, J.; Seo, Y. T.; Zeng, H.; Moudrakovski, I. L.; Ratcliffe, C. I.; Ripmeester, J. A. *Nature* **2005**, *434*, 743–746.

(2) Iversen, B. B.; Palmqvist, A. E. C.; Cox, D. E.; Nolas, G. S.; Stucky, G. D.; Blake, N. P.; Metiu, H. J. *Solid State Chem.* **2000**, *149*, 455–458.

(3) Bobev, S.; Sevov, S. C. *J. Solid State Chem.* **2000**, *153*, 92–105.

(4) Kasper, J. S.; Hagenmuller, P.; Pouchard, M.; Cros, C. *Science* **1965**, *150*, 1713–1714.

(5) Kovnir, K. A.; Shevelkov, A. V. *Uspekhi Khimii* **2004**, *73*, 999–1015.

(6) Pouchard, M.; Cros, C.; Hagenmuller, P.; Reny, E.; Ammar, A.; Menetrier, M.; Bassat, J. M. *Solid State Sci.* **2002**, *4*, 723–729.

(7) Ramachandran, G. K.; Dong, J. J.; Diefenbacher, J.; Gryko, J.; Marzke, R. F.; Sankey, O. F.; McMillan, P. F. *J. Solid State Chem.* **1999**, *145*, 716–730.

(8) Qiu, L. Y.; White, M. A.; Li, Z. Q.; Tse, J. S.; Ratcliffe, C. I.; Tulk, C. A.; Dong, J. J.; Sankey, O. F. *Phys. Rev. B* **2001**, *64*, 02.

(9) Hester, K. C.; Strobel, T. A.; Sloan, E. D.; Koh, C. A.; Huq, A.; Schultz, A. J. *J. Phys. Chem. B* **2006**, *110*, 14024–14027.

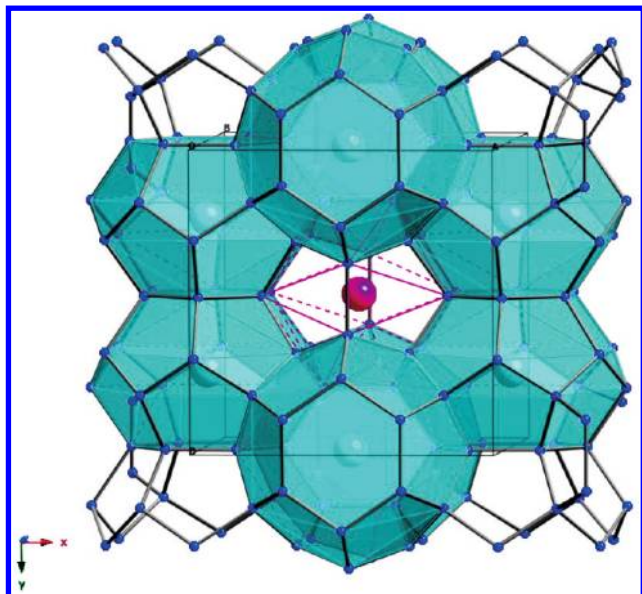


Figure 1. View of the clathrate I structure type down the c axis. The framework atoms are silicon, and the shaded polyhedra are centered by K atoms of the same color in the $6d$ site. The K atom in the $2a$ site is indicated by red, and the red lines provide the outline of the corresponding polyhedra (the K atoms at the corners of the unit cell have been omitted for clarity).

$\text{Na}_{5.5}(\text{H}_2)_{2.15}\text{Si}_{46}$, that encapsulates hydrogen at ambient temperature and pressure from the reaction of Na_4Si_4 with NH_4Br .¹⁰ A clear advantage of inorganic clathrate compounds such as $\text{Na}_{5.5}(\text{H}_2)_{2.15}\text{Si}_{46}$ over their hydrate counterparts is their stability at ambient atmosphere.

Semiconducting clathrate materials are typically synthesized by thermal decomposition of their parent Zintl salts^{3,5,7,11,12} or from elements with the use of high pressure techniques.¹³ Recently, clathrate formation has been reported by reacting Na_4Si_4 with HCl .¹⁴ NH_4X salts provide a convenient acid/oxidation reagent for metal silicides.^{10,15,16} To further explore the ammonium halide as a reagent in the low temperature synthesis of clathrate phases, we have prepared the K-containing Si clathrate. Herein we report the synthesis and characterization of H_2 encapsulated silicon type I clathrate: $\text{K}_{8-x}(\text{H}_2)_y\text{Si}_{46}$.

Experimental Section

1. Synthesis. All manipulations for the synthesis of the potassium silicon clathrate were performed in a N_2 filled glovebox or vacuum/inert atmosphere Schlenk line. Si (99.999% Aldrich) and K (lump 99% Aldrich) were used as received. K_4Si_4 was prepared from K and Si. A 1:1 mixture of the two was welded in a niobium tube, and the niobium tube was sealed in a quartz jacket under a partial argon pressure. The quartz tube was then placed in a furnace and heated with $1\text{ }^\circ\text{C}/\text{min}$ to $650\text{ }^\circ\text{C}$

and dwelled there for 3–4 days. The purity of the obtained K_4Si_4 material was confirmed by powder X-ray diffraction. NH_4Br (99.99% Aldrich) was dried under dynamic vacuum at $100\text{ }^\circ\text{C}$ for 14 h prior to usage. The synthesis of the potassium silicon clathrate was achieved by the solid state reaction between the Zintl salt, K_4Si_4 , and NH_4Br . The optimized reaction consisted of 0.25:0.8 molar ratio, 0.755 g of K_4Si_4 and 0.8825 g of NH_4Br , ground in an agate mortar in a nitrogen filled glovebox and the resulting powder pressed into pellets. The pellets were loaded in a 20 mm long alumina boat and placed in a closed end glass tube with adaptor. The glass tube dimensions must be carefully considered since both ammonia and hydrogen gases are generated in this reaction. The tube was 14.6" long with an internal diameter of $3/4$ " mm, and the adaptor provided an additional 1.5" in length. The tube was connected to a Schlenk line and left under vacuum for 30 min. The tube was then inserted in a furnace preheated at $300\text{ }^\circ\text{C}$ with the sample positioned in the center of the furnace and the adaptor outside of the furnace. The reaction vessel dwelled at $300\text{ }^\circ\text{C}$ for 13 h and then was removed from the furnace and air-cooled to room temperature (RT).

In all reactions, the solid product was determined to be KBr, mainly by X-ray powder diffraction. The salt byproduct is removed by washing first with ethanol and then with warm HPLC grade water. The resulting dark gray powder was dried under flowing argon at $80\text{--}100\text{ }^\circ\text{C}$ overnight.

Caution! Traces of K_4Si_4 spontaneously ignite in air; the products present in the tube have to cool down at RT under vacuum or argon. After the tube is cold it should be disconnected from the Schlenk and allowed to oxidize in air. Only after that the alumina boat should be removed from the glass tube, the products ground into a powder and ethanol addition done slowly. If the product ignites, then the heat from this reaction is sufficient to convert some of the potassium clathrate into silicon.

2. Characterization. Elemental Analysis. Elemental analysis was performed on three different reaction batches by Desert Analytics Laboratories.¹⁷ HF dissolution was requested for the third batch. Elemental analysis results for three batches were as follows.

batch	H	N	Br	K	Si
1	0.4%		1.9%	10%	62.6%
2	0.21%		1.7%	10%	73%
3	0.12%	0.27%	0.1%	14.2%	71%

The variability in composition from sample to sample suggests that the amount of hydrogen may be difficult to control. The total composition is less than 100%, and this is attributed to surface oxidation of the sample, as observed in the TEM,²⁹ ^{29}Si NMR (described below), and FTIR (Supporting Information). If the missing mass is attributed to oxygen and the corresponding Si for SiO_2 is removed, along with assuming that Br is present because of KBr that was not completely removed and the corresponding K was removed, then we arrive at the following K/Si/H ratios: 7.38:46:12.73, 5.07:46:4.5, and 8.0:46:2.63. Averaging these leads to the formula $\text{K}_{6.82}(\text{H}_2)_{3.3}\text{Si}_{46}$. It is possible that the surface oxidation prevents complete dissolution of the sample. It is highly likely that small changes in pressure, temperature, and time provide slightly different average compositions. Therefore, this phase will be referred to as having the general formula $\text{K}_{8-x}(\text{H}_2)_y\text{Si}_{46}$ throughout the manuscript. The microscopy was performed on samples 1 and 2. The solid state NMR, FTIR, and X-ray powder diffraction results were reproduced on all samples. The synchrotron and the TG/DSC/MS data were from sample 3.

EDX/STEM HAADF. Approximately 0.1 g of the synthesized powder has been sonicated for 30 min in n -butanol and spread over a gold-mesh grid covered by a thin perforated

(10) Neiner, D.; Okamoto, N. L.; Condrón, C. L.; Ramasse, Q. M.; Yu, P.; Browning, N. D.; Kauzlarich, S. M. *J. Am. Chem. Soc.* **2007**, *129*, 13857–13862.

(11) McMillan, P. F.; Gryko, J.; Bull, C.; Arledge, R.; Kenyon, A. J.; Cressey, B. A. *J. Solid State Chem.* **2005**, *178*, 937–949.

(12) Sangster, J. *J. Phase Equilib. Diffus.* **2006**, *27*, 190–191.

(13) Tanigaki, K.; Shimizu, T.; Itoh, K. M.; Teraoka, J.; Moritomo, Y.; Yamanaka, S. *Nat. Mater.* **2003**, *2*, 653–655.

(14) Bohme, B.; Guloy, A.; Tang, Z. J.; Schnelle, W.; Burkhardt, U.; Baitinger, M.; Grin, Y. *J. Am. Chem. Soc.* **2007**, *129*, 5348.

(15) Meyer, G. Z. *Anorg. Allg. Chem.* **2008**, *634*, 201–222.

(16) Neiner, D.; Chiu, H. W.; Kauzlarich, S. M. *J. Am. Chem. Soc.* **2006**, *128*, 11016–11017.

(17) <http://www.desertanalytics.com/index.htm>.

carbon film. The grid was heated under dynamic vacuum at 200 °C overnight. Selected area electron diffraction (SAED) and energy dispersive X-ray spectroscopy (EDX) were performed under a JEOL JEM-2500SE electron microscope operated at 200 kV. The sample was also examined using a spherical aberration (Cs) corrected VG HB501 scanning transmission electron microscope (STEM) operated at 100 kV. High-angle annular dark-field (HAADF) images were taken with the convergence semiangle of 20 mrad and collection semiangle of 70–210 mrad, for an estimated probe size of 1.0 Å, sufficient to resolve the 6d and 2a sites of the clathrate in projection.¹⁸ The STEM image simulations were performed using Kirkland's code.¹⁹

Solid State NMR. All Solid-state NMR experiments were performed on a Bruker Avance 500 spectrometer equipped with an 11.75 T magnet. The samples were loaded in Bruker zirconia rotors with kel-F caps in a glovebox filled with dry flowing nitrogen, and TMS was used as the external chemical shift reference. For ¹H MAS NMR, a Bruker 4 mm CP-MAS probe was used with a MAS rate of 15 kHz. A Hahn-echo pulse sequence (90-t-180-acquisition) was used to suppress the signal from the probe background; the 90 degree pulse width was 2.5 μs; the interpulse delay time (*t*) was synchronized with rotor time; the spectrum width was 500 kHz; the relaxation delay was 5 s; a total of 2000 transients was averaged; a block size of 8192 was used and zero-filled to 16384 with 1 Hz line broadening.

For ²⁹Si MAS NMR the sample was loaded in a 4 mm zirconia rotor and a 4 mm Bruker MAS probe was used with a spinning rate of 10 kHz. A Hahn-echo pulse sequence was utilized; the 90 degree pulse length was 2.7 μs, the interpulse delay was synchronized with the rotor time; the spectrum width was 500 kHz; the recycle delay was 300 s; a total of 2006 transients were averaged; the data were processed with 2000 Hz line broadening. For ²⁹Si{¹H} CP MAS NMR experiment, the contact time was 1 ms, the recycle delay time was 5 s, the spectrum width was 250 kHz, the total number of scan was 62206.

FTIR. FTIR data were obtained using a Shimadzu IR Prestige 21 equipped with a diffusive reflectance accessory. The powders were mixed with the KBr using a 1:100 molar ratio dilution of the sample in the KBr matrix. The samples were mixed with KBr in a nitrogen-filled drybox. The FTIR measurements were performed in air.

Powder X-ray Diffraction Data. The powder X-ray diffraction patterns were obtained on a PAD V Scintag instrument (Cu Kα radiation λ = 1.5418 Å) equipped with a graphite monochromator. Data were collected in a step scan mode between 20° and 100° 2θ, with a step size of 0.02°. Structural refinement was done by the Rietveld method with the GSAS package of programs.²⁰ The refined parameters include background, peak shape, cell, atom positions, scale factor, atomic displacement parameters and occupancies. The R-factor (*R_p*), the weighted R-factor (*wR_p*), and the goodness of fit, χ^2 , are defined as follows: $R_p = \sum |y_{io} - y_{ic}| / \sum y_{io}$, $wR_p = [\sum w_i (y_{io} - y_{ic})^2 / \sum w_i (y_{io})^2]^{1/2}$, and $\chi^2 = [wR_p / R_{exp}]^2$, where $R_{exp} = [(N - P) / \sum w_i y_{io}^2]^{1/2}$ and *y_{io}* and *y_{ic}* are the observed and the calculated intensities, *w_i* is the weighting factor, *N* is the total number of observed intensities when the background is refined, and *P* is the number of adjusted parameters.

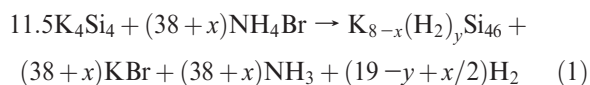
High-resolution powder X-ray diffraction experiments were performed at Stanford Synchrotron Radiation Lightsource (SSRL) on Beamline 2-1. Data were collected in reflection geometry using X-ray energy of 13.5 keV. A Ta-doped Si(111) crystal analyzer was used to define the diffraction beam. Data were collected between 10 and 42 deg 2θ with a step size

of 0.002 deg. The peak profile was chosen to be pseudo-Voigt (Howard asymmetry), and the background was fit to a fifth-order polynomial. Atomic site occupancy and atomic displacement parameters were modeled either by allowing parameters to refine free of manipulation or by setting the model according to the results provided by STEM. The refinement results are provided as Supporting Information.

Differential Scanning Calorimetry (DSC)/Thermogravimetric Analysis (TGA)/Mass Spectrometry (TG/MS). TGA/DSC were performed on a TGA/DSC STA 409 Netzsch instrument by heating the sample under argon. The 409 Netzsch TGA/DSC instrument was coupled with an Aelos QMS 300 MS to identify the evolved gases. The MS utilizes a standard electron impact ionization detector. The transfer line between the TGA/DSC and MS was maintained at 120 °C for the duration of the experiment. The sample was brought under inert atmosphere and loaded in the TGA/DSC/MS instrument. The data were obtained by heating the samples under Ar gas (10 mL/min) from RT to 650 °C with 20 K/min. These particular experimental conditions are necessary to observe low concentrated elements in a sample, for example, low inert gas flow rate and high heating ramp rate. The MS channels observed were mass 2 (hydrogen), 17 (ammonia), 18 (water), 39 (potassium), 40 (potassium hydride), 81 (hydrobromic acid). Only mass 2 and mass 81 channels provided an observable signal over the temperature range measured. The signal for mass 81 occurred at about 50 °C higher than that for mass 2, centered at ~450 °C, and was 2 orders of magnitude weaker than the mass 2 signal under the same MS experimental conditions.

Results and Discussion

A hydrogen-encapsulated potassium silicon clathrate has been synthesized from the solid state reaction of the Zintl salt, K₄Si₄, and NH₄Br. This reaction is heterogeneous and hence complex as it involves both solid and gaseous phases. As with many reactions in the solid state, this reaction is an example of an entropy driven process pushed forward by the evolution of hydrogen, ammonia, and possibly other volatiles. Moreover, the imposed dynamic vacuum helps remove the gaseous phases and hence greatly enhances the rate of the forward reaction. The reaction with molar ratio K₄Si₄/NH₄Br 0.25:1 at 300 °C produces a mixture of potassium silicon clathrate, crystalline silicon, and potassium bromide. However, when the molar ratio K₄Si₄/NH₄Br is changed to 0.25:0.8, the diamond-structure silicon byproduct is avoided, allowing the formation of pure phase type I potassium silicon clathrate and potassium bromide. It is possible that in the case of the slight deficiency of NH₄Br that some of the potassium leaves as K metal, as the reaction is under dynamic vacuum. A general reaction scheme is presented below:



Elemental analysis supports the reaction (1) pathway indicating that hydrogen is present in all samples, and the general formula K_{8-x}(H₂)_ySi₄₆ will be used throughout. In the elemental analysis data sets a small amount of Br was detected. Silicon clathrates encapsulating Cl, Br, and I have been prepared;^{5,21,22} however, the small amount of Br

(18) Krivanek, O. L.; Dellby, N.; Lupini, A. R. *Ultramicroscopy* **1999**, *78*, 1.

(19) *Advanced Computing in Electron Microscopy*; Kirkland, E. J., Ed.; Plenum Press, NY, 1998.

(20) <http://www.ccp14.ac.uk/solution/gsas/>

(21) Kovnir, K. A.; Abramchuk, N. S.; Zaikina, J. V.; Baitinger, M.; Burkhardt, U.; Schnelle, W.; Olenev, A. V.; Lebedev, O. I.; Van Tendeloo, G.; Dikarev, E. V.; Shevelkov, A. V. *Z. Kristallogr.* **2006**, *221*, 527–532.

(22) Yakimchuk, A. V.; Zaikina, J. V.; Reshetova, L. N.; Ryabova, L. I.; Khokhlov, D. R.; Shevelkov, A. V. *Low Temp. Phys.* **2007**, *33*, 276–279.

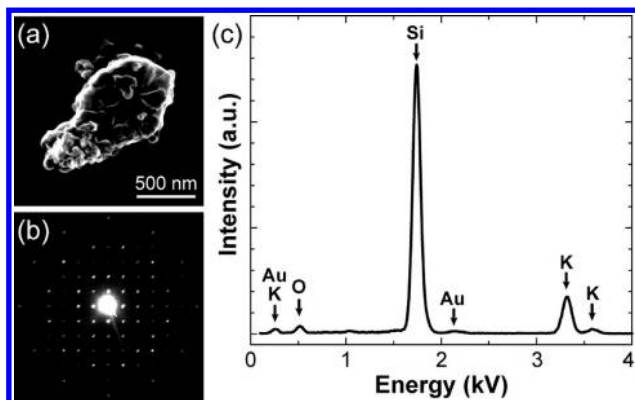


Figure 2. (a) Secondary electron image of a $K_{8-x}(H_2)_ySi_{46}$ clathrate particle. (b) SAED pattern taken along the [100] direction. (c) EDX spectrum of a $K_{8-x}(H_2)_ySi_{46}$ clathrate particle.

observed in the elemental analysis suggests that the Br is probably a result of KBr that was not completely removed by washing, and the quantity is below the detection limit of X-ray powder diffraction. The total weights were consistently lower than 100%, with the highest totals for the elemental analysis observed when HF was employed to dissolve the solid. This suggests that there is an oxide coating on the surface of the powder. These inferences concerning the identity of the Br and the presence of a thin oxide surface are consistent with the microscopy, NMR, and FTIR results, as described below.

Figures 2(a) and 2(b) show a secondary electron image and a SAED pattern of a typical clathrate particle obtained from reaction 1. The SAED patterns observed for the majority of particles examined corresponded to the type I clathrate structure, although an electron diffraction pattern consistent with an amorphous structure was observed for a small number of particles. Figure 2(c) shows an EDX spectrum obtained from the clathrate particle shown in Figure 2(a). No difference was observed between the spectra obtained for shorter and longer acquisition times, indicating that the electron beam did not damage the sample during data acquisition. Only peaks corresponding to Si, K, O, and Au are observed. The Au signature peaks are attributed to the gold-mesh grid supporting the particles. The O peak can be attributed to a thin amorphous layer covering the clathrate particles because a higher O concentration was obtained at a very thin area of the particle. The K content obtained from EDX quantification for eight different particles is 5.5 ± 0.3 per formula unit, when the Si sites are assumed to be fully occupied ($K/Si = 5.5:46$). Further characterization was carried out for this material by HAADF-STEM to determine the K occupancies in the $2a$ and $6d$ sites.

Figure 3 shows raw and low-pass filtered HAADF-STEM images of the potassium silicon clathrate taken along the [100] direction. Since the guest atoms are considered to be weakly bonded to the cage framework,⁵ we anticipated the K guest atoms would be easily damaged by the intense electron probe in the aberration corrected STEM. However, contrary to our expectations, the compound was quite stable, and no beam damage was observed. The ring pattern and the center of the ring correspond to the Si_{24} cage and the $6d$ sites, respectively (the Si_{24} cage with a guest atom is overlaid in Figure 3(b)).

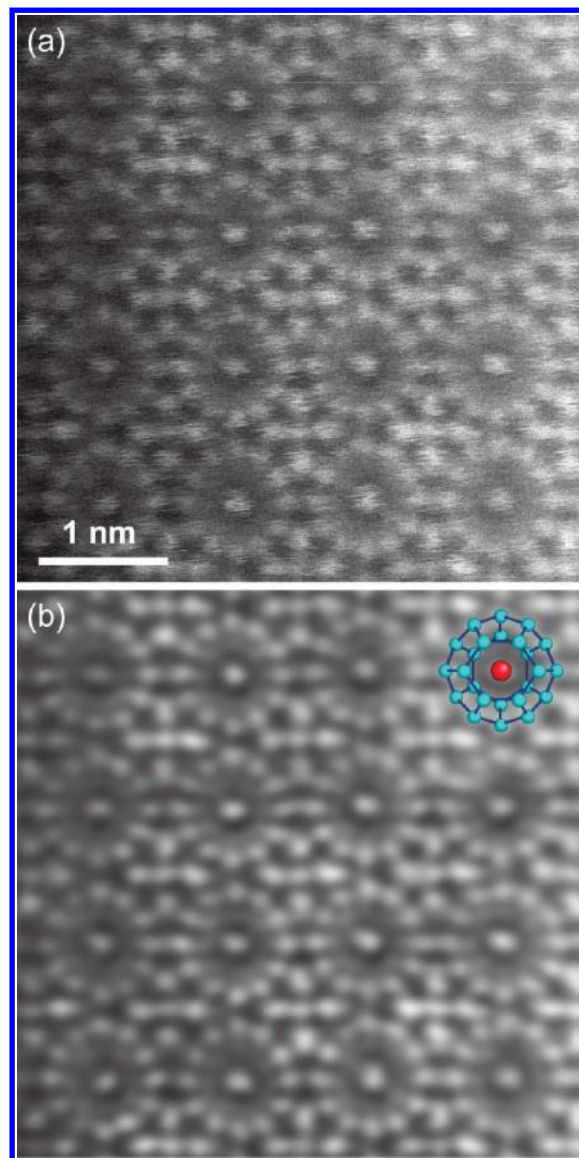


Figure 3. (a) Raw and (b) low-pass filtered HAADF-STEM images of the $K_{8-x}(H_2)_ySi_{46}$ clathrate compound taken along the [100] direction.

Figure 4(a) shows an experimental image averaged by using $2dx$ software and an intensity profile along the yellow line in the image.²³ The image size is one and a half unit cells to allow both the $2a$ and $6d$ sites to be visible in a single image. An intensity peak is observed at the $6d$ site, whereas a dip is seen at the $2a$ site. Figures 4(b)–(e) show calculated images and intensity profiles with different K occupancies in the $2a$ and $6d$ sites. The intensities at the $2a$ and $6d$ sites decrease with the decreasing K occupancies: the intensity of HAADF-STEM images is indeed proportional to the n^{th} power Z^n ($n = 1.5-2$) of the average atomic number Z of the material being observed, and they are therefore often referred to as Z -contrast images.^{24,25} The best way to estimate occupancies from STEM-HAADF is to compare the integrated intensities at the sites. The peak width at the $6d$ site in Figure 4(a) [experiment] is broader than that in Figure 4(d) [$6d = 0.8$].

(23) Renault, L.; Chou, H. T.; Chiu, P. L.; Hill, R. M.; Zeng, X. Y.; Gipson, B.; Zhang, Z. Y.; Cheng, A. C.; Unger, V.; Stahlberg, H. *J. Comp.-Aided Mol. Des.* **2006**, *20*, 519–527.

(24) Jesson, D.; Pennycook, S. J. *Proc. R. Soc. London* **1995**, *A 449*, 273.

(25) Hatrel, P.; Rose, H.; Dinges, C. *Ultramicroscopy* **1996**, *63*, 93.

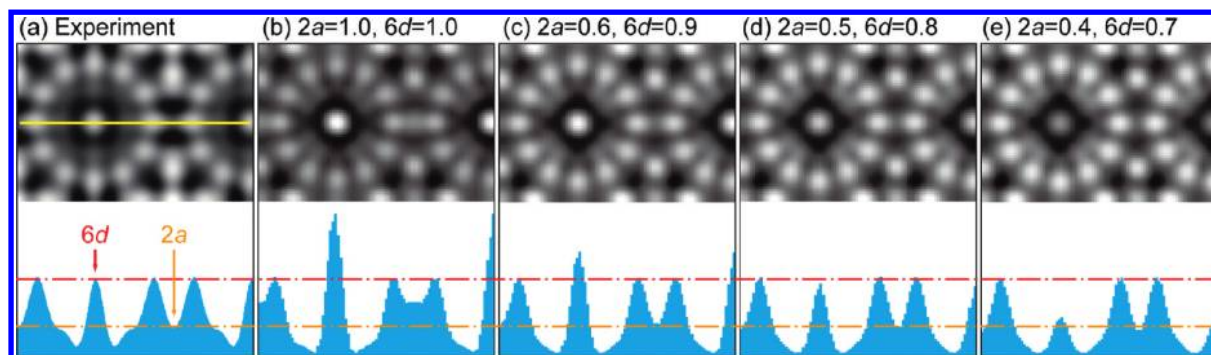


Figure 4. (a) Experimental HAADF-STEM image averaged by using the *2dx* software and intensity profile along the yellow line indicated in the image. (b)–(e) Simulated images with different potassium occupancies at the *2a* and *6d* guest sites and their intensity profiles.

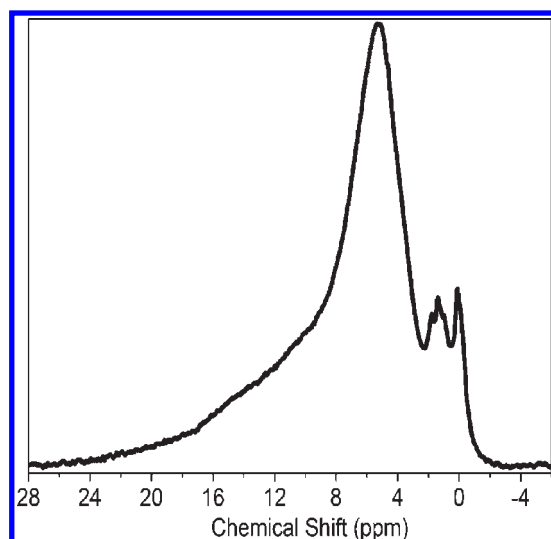


Figure 5. Magic angle spinning ^1H solid state NMR spectrum for $\text{K}_{8-x}(\text{H}_2)_y\text{Si}_{46}$.

The broadening comes from thermal vibration of atoms and sample vibration during the observation. When integrated intensities were compared, the occupancy is larger: the *6d* site is 0.9 and the *2a* site is 0.6. Thus, the overall K content obtained with the HAADF-STEM image is approximately 6.6 per unit formula, which is slightly larger than the EDX result (5.5). The K content from HAADF-STEM image provides the analysis for one particle, whereas the EDX is for a larger sample size; however, the errors should be less in the HAADF-STEM image.

^1H MAS NMR spectrum is presented in Figure 5. There are five distinct resonances in the proton NMR spectrum at 5.26 ppm, 1.8 ppm, 1.4 ppm, 0.94 ppm, and 0.05 ppm. The data show that hydrogen is present in this material; however, the structure of the spectrum differs from that reported for $\text{Na}_{5.5}(\text{H}_2)_{2.15}\text{Si}_{46}$.¹⁰ In the case of $\text{Na}_{5.5}(\text{H}_2)_{2.15}\text{Si}_{46}$ clathrate, there were also five distinct resonances in the ^1H NMR spectrum at 4.2 ppm, 3.8 ppm, 1.3 ppm, 0.79 ppm and 0.08 ppm, with the largest resonance at 4.2 ppm.¹⁰ The resonance at 4.2 ppm was attributed to H_2 encapsulation in the large Si_{24} cage, based on evaluation of similar assignments for a type II $\text{THF}\cdot\text{H}_2\text{O}$ clathrate.²⁶ There is a downfield shift of the hydrogen resonance in $\text{K}_7(\text{H}_2)_3\text{Si}_{46}$ as compared to

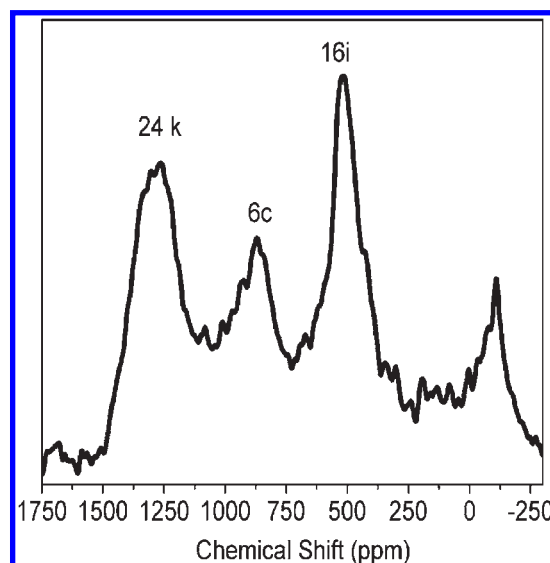


Figure 6. Magic angle spinning ^{29}Si solid state NMR spectrum for $\text{K}_{8-x}(\text{H}_2)_y\text{Si}_{46}$.

$\text{Na}_{5.5}(\text{H}_2)_{2.15}\text{Si}_{46}$. The broad resonance observed in Figure 5 at 5.26 ppm is consistent with H_2 that has restricted motion and may be interacting with both cages. The assignment of these peaks to H_2 molecules rather than H covalently bound to Si is consistent with the absence of any Si–H stretches in the FTIR and the lack of a signal in $^{29}\text{Si}\{^1\text{H}\}$ CP MAS NMR. It is possible that the resonance at 5.26 ppm observed in the ^1H NMR is a result of H_2 in both cages in varying amounts, and hence moved to lower fields compared with that observed for the $\text{Na}_{5.5}(\text{H}_2)_{2.15}\text{Si}_{46}$ ^1H spectrum. This hypothesis would also be consistent with the HAADF-STEM analysis presented herein indicating that both *2a* and *6d* sites are partially occupied in the H_2 encapsulated potassium clathrate while only the *6d* sites are partially occupied in the sodium compound.¹⁰

^{29}Si MAS NMR is presented in Figure 6 and shows four resonances at 1274, 886, 509, and -74 ppm; three are attributed to the clathrate framework and one at -74 ppm is attributed to oxide. The chemical shifts for the three resonances are similar to those published for $\text{K}_{7.66}\text{Si}_{46}$ prepared by vacuum decomposition of the binary silicide, KSi , at elevated temperatures (1384, 940, and 556 ppm),²⁷ but shifted

(26) Florusse, L. J.; Peters, C. J.; Schoonman, J.; Hester, K. C.; Koh, C. A.; Dec, S. F.; Marsh, K. N.; Sloan, E. D. *Science* **2004**, *306*, 46C9–471.

(27) Ferguson, M. J.; Moudrakovski, I. L.; Ratcliffe, C. I.; Tse, J. S. *Mat. Res. Soc. Symp.* **2002**, *691*, G14.4.1–G 14.4.6.

to higher shielding field and broader. In reference 27, it was noted that the resonance at 940 ppm showed a distinct anisotropy and therefore was best assigned to the Si in the 6*c* site. The higher shielding field and broader resonances for $K_{8-x}(H_2)_ySi_{46}$ may be attributed to relative K depletion and local disordering in our sample compared with the stoichiometric samples prepared by vacuum decomposition.

Similar to previously published assignments for $K_{7.66}Si_{48}$, the broad feature at 509 ppm has been assigned to the 16*i* Si site, and the signals at about 1274 and 886 ppm are for Si in 24*k* and 6*c* sites.²⁷ The broad feature of the signal for Si 24*k* compared with Si 16*i* indicates that K 6*d* sites are more disordered than K 2*a*. Therefore the composition of the guest species inside this cage is more variable. This result is consistent with the relatively larger displacement parameter in XRD (discussed below) and HAADF-STEM data. Our ²⁹Si MAS NMR spectrum shows different intensities for these resonances compared with reference 27. While there is no detailed information about the previously published NMR experiments, we speculate that the difference could be due to the following reasons: first, the recycle delay might not be long enough; with 300 s recycle delay, it might saturate some signals with long *T*₁ relaxation times. Second, the Hahn-echo pulse sequence used in our experiment might cause the loss of some broad signals. Although the relative intensities of our NMR data are different than those in the literature, the peak positions are consistent with the published assignments and provide strong evidence about the presence of these cages in clathrate structure.²⁷ The ²⁹Si NMR spectrum is quite different for the potassium clathrate as compared with the sodium clathrate, suggesting the conduction electron density is higher in this Si framework as compared to the Na analogue.^{10,27} The Na atoms in the cages of clathrate are considered nearly neutral, with a small amount of electron transfer to the framework, and the 3*s* electrons cause the strong Knight shift observed for the Si in the framework structure.²⁸ K has more electrons and therefore is more metallic than sodium; the depleted K atoms in the 6*d* and 2*a* cages would cause a stronger Knight shift than the Na analogue. This is consistent with what is observed for the rubidium clathrate where the positions and line widths of the ²⁹Si NMR signals are even more different than the sodium clathrate.²⁷ Introduction of Ba in sodium clathrate also causes broadening, shifts, and intensity changes in ²⁹Si NMR,²⁹ providing further support for our spectral assignments.

The resonance at -74 ppm is very close to -100 ppm which is the normal Si-O resonance, and it may be assigned to oxidation of the surface.²⁸⁻³⁰ This observation is further supported by our EDX data, in which oxygen was detected; however, amorphous silica has not been observed by X-ray diffraction and thus it is most likely present as a thin oxide coating rather than amorphous SiO₂ (see Figure 7 and synchrotron data in Supporting Information).

²⁹Si{¹H} CP MAS NMR spectrum showed no resonance consistent with the absence of a Si-H bond. The ²⁹Si{¹H} spectrum is presented in the Supporting Information. FTIR

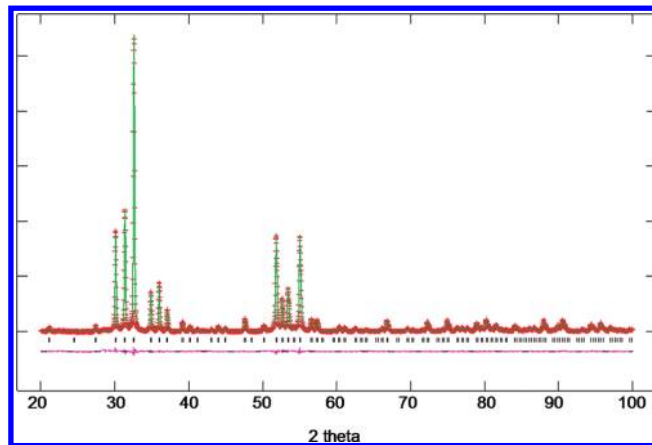


Figure 7. Rietveld profile fit for $K_{8-x}(H_2)_ySi_{46}$ ($\lambda = 1.5418 \text{ \AA}$). Calculated (solid green line), experimental (red crosses) and the difference (lower magenta line). The data were refined for the space group $Pm\bar{3}n$.

analysis on the solid sample also indicated that there is no Si-H stretch present, consistent with the proposed encapsulation of H₂ rather than a hydride. The FTIR data are provided in the Supporting Information.

Laboratory and synchrotron X-ray data were collected on $K_{8-x}(H_2)_ySi_{46}$ obtained in this study. The synchrotron data confirms the clathrate structure and absence of significant amounts of amorphous SiO₂ (Supporting Information). The refined lattice parameter obtained was $a = 10.266(2) \text{ \AA}$. The X-ray powder diffraction data along with the Rietveld refinement are presented in Figure 7. The diffraction peaks were indexed to a cubic cell, space group $Pm\bar{3}n$, $a = 10.2932(3) \text{ \AA}$, slightly larger than that obtained from the synchrotron data refinement and reported for K_8Si_{46} ($a = 10.27518(5) \text{ \AA}$), prepared via high temperature decomposition of K_4Si_4 .⁷

Atomic site occupancies were modeled according to the occupancy obtained by HAADF-STEM. In this case the refinement did not improve beyond a $\chi^2 \sim 5$, and the difference map indicated discrepancies between the calculated and the observed powder patterns. Three approaches were taken to refine the model. In all these approaches the Si and K 2*a* sites were fully refined, for example, atomic positions, site occupancies, and displacements. In one approach the atomic displacement of K in the 6*d* site was fixed to be similar to all the other atoms and the occupancy of the site was refined. This produced an improved fit of the experimental with the observed powder patterns; the occupancy of the 6*d* site decreases, but the refinement was not stable and did not converge. Moreover, opening the displacement flag for the K 6*d* site caused the displacement parameter to increase to 3.0, double those for the other atoms. The second approach was to consider an anisotropic displacement on the K 6*d* site. It is known that anisotropic displacements are not adequate with X-ray powder diffraction data,³¹ however; because this has been employed with K_8Si_{46} , a similar approach was explored here. It was found that the displacement for this site did not improve beyond $U_{11} = 2.2$ and $U_{22} = U_{33} = 3.4$, while $U_{12} = U_{13} = U_{23} = 0$. A third approach was to move K from the center of the Si₂₄ cage, the 6*d* site, to an off-center position in the 24*k* site (0.24, 0.51, 0). This has been proposed before by Tse to model the changes in

(28) Gryko, J.; McMillan, P. F.; Sankey, O. *Phys. Rev. B* **1996**, *54*(5), 3037-3039.

(29) Shimizu, F.; Maniwa, Y.; Kume, K.; Kawaji, H.; Yamanaka, S.; Ishikawa, M. *Synth. Met.* **1997**, *86*, 2141-2142.

(30) Onischuk, A. A.; Strunin, V. P.; Samoilova, R. I.; Nosov, A. V.; Ushakova, M. A.; Panfilov, V. N. *J. Aerosol Sci.* **1997**, *28*, 1425-1441.

(31) McCusker, L. B.; Von Dreele, R. B.; Cox, D. E.; Louer, D.; Scardi, P. *J. Appl. Crystallogr.* **1999**, *32*, 36-50.

Table 1. Crystallographic Refinement Data for the $K_{8-x}(H_2)_ySi_{46}$ Clathrate Phase, Space Group $Pm\bar{3}n^a$

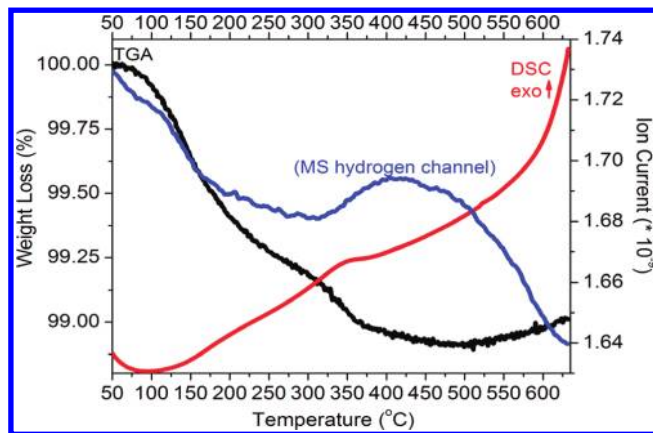
atom	Wyckoff	x	y	z	occupancy	100*U _{iso} (Å ²)
K	2a	0	0	0	0.834(6)	1.6(0)
K	6d	0.25	0.5	0	0.965(4)	3.0(6)
Si	24k	0	0.3067(8)	0.1183(8)	1	1.5(3)
Si	16i	0.1842(6)	0.1842(6)	0.1842(6)	1	1.4(1)
Si	6c	0.25	0	0.5	1	1.3(2)

^a Lab X-ray source, 8.75 keV. $a = 10.2932(3)$ Å, $R_p = 3.34\%$, $R_{wp} = 4.49\%$, $\chi^2 = 2.933$.

the K_8Si_{46} crystal structure at high pressures.³² In doing so, the isotropic displacement improved, 2.0, and the occupancy was 0.25 for the K in a 24k site, which gave the overall composition $K_{7.6}Si_{46}$.³² The refinement presented in Figure 7 and the cell parameter and atomic positions presented in Table 1 are provided for the model where all sites refine freely, and the occupancies for the K were allowed to vary while those of Si were fixed. This corresponds to the stoichiometry, $K_{7.5}Si_{46}$, consistent with the refinement of the structure of potassium silicon clathrate prepared by other methods.⁷ It is known that the occupancy, displacement, and the scale factor are highly correlated, and can be very difficult to refine with X-ray powder diffraction data.³¹

Theoretical calculations for an empty Si_{46} framework indicate that the minimum energy configuration is obtained for $a = 10.355$ Å,³³ and $K_{7.6}Si_{46}$ prepared by vacuum decomposition of K_4Si_4 has a smaller lattice parameter of 10.2751 Å.¹² The samples presented herein show lattice parameters slightly larger to slightly smaller than that reported for $K_{7.6}Si_{46}$. This suggests that encapsulation with K, or any other guest provides some interaction with the framework. There seems to be variation in exact stoichiometry in the sample. It is possible that while all the sample is type I clathrate, there is inhomogeneity that leads to different lattice constants. The K atom, refined in the 6d site, had a large displacement parameter, almost double the other atoms in the structure. This large displacement parameter could indicate significant variability in composition for this site. If H_2 shares this site, this may also contribute to the large displacement parameter. These factors make it difficult, without very high resolution data, to obtain accurate occupancy for the K on the 6d site by refinement of X-ray powder diffraction data.

While elemental analysis, EDX, and HAADF-STEM suggest a lower K content than the X-ray refinement where the average K occupancy results in a stoichiometry closer to 7.5, although the larger lattice parameter and displacement parameter for K in the 6d site may indicate that the powder X-ray data is not of high enough quality to provide a definitive model of the guest site and an accurate stoichiometry. One cause of the discrepancy observed between the elemental analysis, EDX, and HAADF-STEM on one hand and the X-ray data on the other is the respective sample sizes used by these techniques. While the elemental analysis and microscopy used 10–20 mg, our X-ray experiment used 0.5–1 g of the same sample and therefore should provide a more accurate average for the sample. Moreover, the STEM

**Figure 8.** TGA/DSC/MS data for $K_{8-x}(H_2)_ySi_{46}$. Traces are as indicated on the figure. TG curve is black, DSC curve is red, and hydrogen MS signal is shown in blue.

results indicate that the sample is not homogeneous, that is, K content not only varies from one unit cell to another, but it is possible that some parts of the sample are K-rich while others are K-deficient. As STEM is not dependent upon the average, this provides a local composition and structure information. This variability is probably induced through the processing, as H_2 may be encapsulated as a gas and K is removed from the silicide as the salt, KBr, with concomitant clathrate formation. X-ray diffraction not only analyzes a larger sample size but also provides the average K and Si occupancies. Chemical analysis for the three samples measured also suggests variability in stoichiometry, and further efforts at controlling pressure may result in a more well-defined sample composition.

The TGA/DSC/MS data are presented in Figure 8. The TGA data show a weight loss of ~1.1% that occurs above 100 °C; the DSC data show a very broad exotherm at ~350 °C, and a broad and weak MS signal, hydrogen channel, at ~400 °C. K or KH are not observed in the MS, in agreement with the reported high thermal stability of potassium type I silicon clathrate. The sample did not decompose during heating under these conditions. Potassium clathrate, K_8Si_{46} , is reported to be stable at higher temperatures than its sodium analogue.³² It has been experimentally seen by us and others that sodium type I clathrate decomposes to diamond-structured silicon upon heating at 20 K/min to 650 °C, potassium type I clathrate maintains its cage-like structure under the same experimental conditions. An X-ray diffraction pattern of samples after the above-mentioned heat treatment shows crystalline Si in the case of sodium clathrate and leaves the potassium silicon clathrate almost unchanged.

Summary

The presence of hydrogen is provided by elemental analysis, 1H MAS NMR, and TG/MS. FTIR and $^{29}Si\{^1H\}$ CP MAS NMR show no evidence for Si–H bonds, suggesting that the hydrogen is molecular in nature, and not bonded to the silicon framework. These results are consistent with a model of H_2 entrapped in the guest site. HAADF-STEM provides detailed structural information as to the framework structure and guest site occupancy suggesting that the solid is inhomogeneous and that at least some of the clathrate is deficient in K. This model is further supported by ^{29}Si MAS NMR. Rietveld refinement of the X-ray diffraction data provides an averaged structure where K in the 6d site has a

(32) Tse, J. S.; Desgreniers, S.; Li, Z. Q.; Ferguson, M. R.; Kawazoe, Y. *Phys. Rev. Lett.* **2002**, *89*(19), 195507-1–195507-4.

(33) Adams, G. B.; Okeeffe, M.; Demkov, A. A.; Sankey, O. F.; Huang, Y. M. *Phys. Rev. B* **1994**, *49*, 8048–8053.

doubled displacement parameter with respect to the other atoms in the refinement, suggesting variability in composition for the hydrogen encapsulation clathrate, $K_{8-x}(H_2)_ySi_{46}$. Further investigation of the synthesis with ammonium salt along with *in situ* measurements would provide insight into the formation of this hydrogen encapsulated inorganic clathrate.

Acknowledgment. The authors gratefully acknowledge Dr. Alexandra Navrotsky for use of the powder diffractometer. We wish to thank David G. Morgan, who carried out the image processing using *2dx* software. This work was supported by the Center of Excellence for Chemical Hydrides under Contract No. DE-FC36-05GO15055, by the Department of Energy under Con-

tract No. DE-FG02-03ER46057, and by the Japan Society for the Promotion of Science for Young Scientists. Part of this work was carried out at the National Center for Electron Microscopy, under the auspices of the U.S. Department of Energy under contract number DE-AC02-05CH11231. Portions of this research were carried out at the Stanford Synchrotron Radiation Lightsource, a national user facility operated by Stanford University on behalf of the U.S. Department of Energy, Office of Basic Energy Sciences.

Supporting Information Available: Spectra of the $^{29}Si\{^1H\}$ CP MAS NMR and FTIR, Rietveld refinement of the synchrotron data. This material is available free of charge via the Internet at <http://pubs.acs.org>.